Desalination and Water Treatment
www.deswater.com

doi: 10.5004/dwt.2017.0334

60 (2017) 200–211
January

Amino-functionalized bimodal ordered mesoporous carbon with high surface area for efficient adsorption of lead (II) ions

Kunquan Li[a], Zeqing Wan[a], Jun Li[b], Mingzhou Lu[a,*], Xiaohua Wang[a]

[a]*College of Engineering, Nanjing Agricultural University, Nanjing 210031, China, Tel. +86-25-58606630; Fax: +86-25-58606573; email: kqlee@njau.edu.cn (K. Li); Tel. 025-25-58606630; Fax: +86-25-58606573; email: 247057626@qq.com (Z. Wan); Tel. +86-25-58606573; Fax: +86-25-58606573; email: 2381998179@qq.com (M. Lu); Tel. +86-25-58606574; Fax: +86-25-58606573; email: xhwang@njau.edu.cn (X. Wang)*
[b]*School of Environmental Science and Engineering, Zhejiang Gongshang University, Hangzhou, Zhejiang, 310012, China, Tel. +86-25-58606574; Fax: +86-25-58606573; email: lijun681116@sina.com*

Received 24 March 2016; Accepted 20 July 2016

ABSTRACT

A co-assembled stable bimodal-ordered mesoporous carbon (CBOMC) with high surface area was synthesized via a simple, low-costing, and easily reproducible method, and subsequently modified with ammonium peroxydisulfate and diethylenetriamine (APD) to develop an amino-rich adsorbent (CBOMC-APD) for Pb(II) removal. Nitrogen adsorption/desorption data suggested that the bimodal-ordered mesostructural regularity was well-reserved after surface amination. X-ray photoelectron spectroscopy (XPS) and Fourier transform infrared spectroscopy analyses indicated that the amino groups were chemically bound to CBOMC-APD. The influences of solution pH, initial concentration, adsorbent dose, temperature, and contact time on adsorption were investigated in detail. The CBOMC-APD exhibited excellent adsorption performance for Pb(II). The adsorption capacity reached 391 $mg \cdot g^{-1}$, and almost 80% of Pb(II) was removed in 30 min. The Pb(II) combined with the amino groups through strong complexation based on the comparison of XPS analyses before and after adsorption, which endowed it with significant adsorption capacity and high pH stability. The adsorption mechanism study suggested that the mesopore structures and amino groups considerably contributed to the high adsorption rate and adsorption ability, respectively. High adsorption capacity, kinetic rate, and reusability indicated that the amino-rich bimodal CBOMC-APD with high surface area has great potential as a new adsorbent for Pb(II) removal.

Keywords: Bimodal-ordered mesoporous carbon; Amino modification; Lead ion; Ammonium peroxydisulfate; Mesostructural regularity

1. Introduction

Heavy metal ions in water pose a potential threat to aquatic lives and humans because of their accumulation in the food chains [1]. Lead, a ubiquitous heavy metal pollutant in the natural water environment, arises from industrial processes, such as electroplating, alloy manufacturing, pigments, batteries, and textile operations [2,3]. The presence of excessive lead in drinking water causes anemia, encephalopathy, and hepatitis, among others [4]. It can also damage the kidney, liver, reproductive system, basic cellular processes, and brain functions [5]. Methods, such as chemical precipitation, membrane filtration, adsorption, electrochemical treatment technologies, biochemical methods, and biological ion exchange, are used to remove heavy metal ions from wastewaters [6–9]. Adsorption is regarded as a highly effective treatment method to remove heavy metal ions from wastewaters because of its ease of use, low cost, and environmental viability. Porous materials, such as activated carbon, zeolite, clay, kaolinite, and silica gel, have been employed extensively to remove heavy metals from aqueous solution [10–13].

* Corresponding author.

Ordered mesoporous carbon (OMC) with large surface area, uniform bimodal pore connections and high pore volume has received increasing attention because of its unprecedented adsorption performance toward a wide range of inorganic and organic chemicals [14,15]. It is well known that the pore properties and surface chemical groups of carbon materials are two crucial factors, which greatly influence the adsorption performances of heavy metals. In order to further enhance the adsorption abilities of carbon materials for various metal ions, more recent researches have been focused on introducing heterocyclic chemical functional groups containing oxygen, nitrogen, or sulfur atom on the exterior surface or internal pore surface of carbon materials. Our recent research [16,17] reported that the oxygen and nitrogen-containing mesoporous carbon showed much higher adsorption capacity for lead ions, and the strong adsorption capacity was mainly attributed to the existence of mesoporous structure and the electron-donating effect of the incorporated nitrogen-containing functional groups.

Amino modification is a promising method for enhancing the adsorption efficiency of metal ions on carbon materials because amino moiety is a powerful complexing functional group that efficiently complexes with heavy metals due to the high stability constants of the metal complexes properties [18–23]. A few recent works showed that amino-modified mesoporous carbons have strong ability for the adsorption of metal ions in wastewater [21–23]. Several methods have been carried out to introduce amino groups on carbon surfaces, including the reduction of a nitro group formed by a HNO_3/H_2SO_4 mixture, reaction with carboxyl groups introduced by acid treatment with diamine compounds, and treatment with gaseous ammonia [22,24–26]. However, the surface amino modification reaction can destroy the ordered array of OMC, and even decrease the pore volume. For instance, Mariusz Barczak reported that the porosity of SBA-15 templated OMC CMK-3 diminished significantly after oxidized treatment with $(NH_4)_2S_2O_8/H_2SO_4$ and amino-functionalized treatment with N-(3-trimethoxysilylpropyl)diethylenetriamine though the adsorption capacity of the carbon for lead ions was improved [27].

Moreover, researches on surface chemistry modification of OMCs have mostly focused on that of the CMK-type carbon replica prepared by nanocasting [27–30]. However, for the OMC prepared from a facile tri-constituent co-assembly method, there are limited relevant studies. Compared with the CMK-type counterpart, these series of assembled OMCs exhibit greatly improved stability of the mesopore regularity under surface chemistry modification because of the intrinsic structural advantages covalently bonded carbon construction, 3D amorphous carbon open frame-work and thick pore walls. Recently, Zhao groups reported a simple, low-costing, and easily reproducible method to prepare highly stabilized OMC-silica nanocomposites with "reinforced-concrete"-like structures by a tri-constituent co-assembly strategy using resols and prehydrolyzed TEOS as organic and inorganic precursors and triblock copolymer F127 as templates via the EISA approach [31]. After silica was etched from the OMC-silica nanocomposites by NaOH solution, the co-assembled bimodal ordered mesoporous carbon (CBOMC) can be obtained. The CBOMC features more stability, high surface area, bimodal pores and plenty of small pores in carbon pore walls.

Herein, we present a comprehensive study on the surface chemistry and textural property of the CBOMC with high surface area and bimodal pores by amination treatment, and the adsorption behavior toward Pb(II) in aqueous solutions. The CBOMC was synthesized via a tri-constituent co-assembly strategy using resols and prehydrolyzed TEOS as organic and inorganic precursors and triblock copolymer F127 as templates, and subsequently amino-functionalized by treatment with ammonium peroxydisulfate and diethylenetriamine (APD). The mesostructure and pore evolution of the pristine CBOMC and amino-modified CBOMC (CBOMC-APD) were examined by small-angle X-ray diffraction (SAXRD), transmission electron microscope (TEM) and N_2 adsorption-desorption measurement. Species distribution and quantitative information of the nitrogen-containing functional groups were obtained based upon a detailed X-ray photoelectron spectroscopy (XPS) analysis through the deconvolution of high resolution C1s/N1s spectra. The adsorption behavior of the CBOMC-APD toward Pb(II) was fully investigated, showing an extremely fast kinetics and an adsorption isotherm in accordance with the Langmuir model. The elution of the complexed Pb(II) was achieved for the regeneration of the amino-rich bimodal ordered mesoporous CBOMC-APD.

2. Materials and methods

2.1. Reagents and apparatus

High-purity nitrogen (99.999%) was purchased from the head office of MII 55 Institute. Analytically pure chemical reagents, such as ammonium peroxydisulfate, diethylenetriamine, absolute ethyl alcohol, dicyclohexylcarbodiimide (DCC), and lead nitrate, were purchased from Shanghai Chemical Reagent Co., Ltd. Pluronic F127 (Mw = 12,600, $EO_{106}PO_{70}EO_{106}$) was supplied by Sigma-Aldrich. Micromeritics ASAP-2020 analyzer (Micromeritics, USA); CHN-O-Rapid elemental analyzer (Heraeus Co., Germany).

2.2. Preparation of CBOMC

Pristine CBOMC was prepared by EISA, a typical soft template method invented by Zhao et al. [31]. Firstly, a resol precursor was synthesized through polymerization reaction between phenol and formaldehyde in alkaline condition. Phenol (6.1 g) was melted at 40°C–42°C in a flask and mixed with 1.3 g of 20 wt% NaOH aqueous solution while stirring. After 10 min, 10.5 g of formalin (37 wt% formaldehyde) was added dropwise below 50°C. After continuous stirring for 1 h at 70°C–75°C, the mixture was cooled to room temperature and the pH value was adjusted to about 7.0 using HCl solution. Afterward, water was removed by vacuum evaporation below 50°C, and the final product was dissolved in ethanol (20 wt% ethanolic solution). Eventually, ethanol solution of resol was obtained.

Secondly, carbon-silica nanocomposites were prepared by tri-constituent co-assembly of resols, oligomer silicates from tetraethyl orthosilicate (TEOS), and tri-block copolymer F127 template. In a typical preparation, 1.6 g of block copolymer F127 was dissolved in 8.0 g of ethanol with 1.0 g of 0.2 M HCl. The mixture was stirred for 1 h at 40°C until a

clear solution was achieved. Next, 2.08 g of TEOS and 5.0 g of 20 wt% resol ethanolic solution were added in sequence. The mixture was stirred for 2 h and then transferred to dishes. The ethanol was evaporated for 5–8 h at room temperature and for 24 h at 100°C in an oven for thermopolymerization. The as-made products, flaxen and transparent films or membranes were scraped from the dishes and ground into fine powder. Calcination was carried out in a tubular furnace at 350°C for 3 h and at 900°C for 2 h under N_2 flow, with a heating rate of 1°C·min^{-1} below 600°C and 5°C·min^{-1} above 600°C. Then, the products were cooled in the inert atmosphere and ground to obtain the carbon-silica nanocomposites. Finally, the produced carbon–silica nanocomposites were immersed in 4 M NaOH solutions for 24 h to remove the silica and obtain the CBOMC.

2.3. Modification of CBOMC

Ten grams of the as-received CBOMC was added to the flask containing 600 mL of 1 mol L^{-1} ammonium peroxydisulfate (APS, prepared by 2 mol L^{-1} H_2SO_4), stirred for 20 min, and heated to 60°C. After 20 h of reaction, the mixture was cooled to room temperature. The black powder was collected by vacuum filtration and washed repeatedly with water and ethanol until no precipitation was created when adding barium nitrate onto the filtrate. The oxidized CBOMC was dried in a vacuum oven at 80°C for 48 h. Afterward, 5.0 g of oxidized CBOMC, 150 mL of diethylenetriamine (DEA), and 5.0 g of DCC were placed in a 250 mL flask equipped with a mechanical stirring device and a reflux condenser. After 48 h of reflux at 120°C, the product was separated by filtration and washed repeatedly with ethanol and ether. The desired product was dried at 80°C for 8 h, and the APS and DEA-modified CBOMC (CBOMC-APD) was derived.

2.4. Characterizations

The ordered degree of pore channels of the prepared CBOMC was measured by SAXRD (X'Pert Pro DY2189; PANaytical, B. V., Netherlands) using Cu-K radiation. Inner textural images of the samples dispersed in ethanol were obtained by transmission electron microscopy (TEM) (JEM-200CX; JEOL Ltd., Tokyo, Japan) at an accelerating voltage of 120 kV. The carbon, hydrogen, and nitrogen percentage contents of the carbons were analyzed by a CHN-O-Rapid elemental analyzer (Heraeus Co., Germany). Nitrogen adsorption isotherms were obtained with N_2 at 77 K after degassing the carbons at 150°C under N_2 atmosphere for 3 h. The surface area was calculated by Brunauer–Emmett–Teller (BET) model, and the pore size distribution was calculated from N_2 adsorption data using the nonlocal density functional theory equilibrium model method for slit pores. Total pore volume was obtained by converting the nitrogen adsorption amount at a relative pressure of 0.98 to the liquid nitrogen volume. The mesopore volume (V_{BJH}) was deduced using the Barrett–Joyner–Halenda method. Bruker Tensor 27 type Fourier-transform infrared spectrometer was employed to determine the identity of surface functional groups. PHI 5000 Versa Probe X-Ray electron spectrometer from Ulvac-Phi was used to acquire the XPS images of the carbons before and after Pb(II) adsorption.

2.5. Adsorption experiments

2.5.1. Effect of pH

The prepared adsorbents (CBOMC-APD and CBOMC) were used to study the effect of pH on Pb(II) ion adsorption. Effects of pH (1.5–6.5) experiments were studied in 200 mL Pb(II) solutions with the initial concentration of 20 mg·L^{-1} by contacting 0.015 g of adsorbents for 24 h at a temperature of 25°C. The desired pH of the suspensions in each flask was adjusted using 0.01 mol·L^{-1} HNO_3 or NaOH solution. All the adsorption tests were carried out in triplicate to confirm reproducibility of the experimental results. The reproducibility and relative standard deviation (RSD) are less than 5%.

2.5.2. Effect of temperature

The effect of temperature was investigated in 200 mL Pb(II) solutions at pH 4.5 with initial Pb(II) concentrations ranging from 3 to 70 mg·L^{-1} by contacting 0.015 g of CBOMC-APD for 24 h at different temperatures of 25°C, 35°C, and 45°C. For comparison, the Pb(II) adsorption on the pristine CBOMC was also investigated at 25°C under the same conditions. The amount of Pb(II) ions bound by the adsorbent was calculated as follows:

$$q_e = (C_0 - C_e)\, V/W \tag{1}$$

where C_0 (mg·L^{-1}) is the initial Pb(II) ion concentration, C_e (mg·L^{-1}) is the Pb(II) ion concentration at the equilibrium liquid phase, V (L) is the volume of the solution, and W (g) is the mass of adsorbent used.

2.5.3. Kinetics experiment

Kinetics experiments were conducted by shaking the flasks at 25°C in different contact times (0–4 h). For each experiment, 0.075 g of adsorbent was added to 1000 mL of Pb(II) ion solution with different initial concentrations of 10, 20, and 30 mg·L^{-1} (pH of the Pb(II) solution was adjusted to 4.5). Metal ion concentrations were measured using an atomic adsorption spectrophotometer (AA-6300; Shimadzu, Japan).

2.6. Desorption and reusability studies

The CBOMC-APD was first saturated with Pb(II) by placing 0.1 g adsorbent in 200 mL of 20 mg L^{-1} Pb(II) solution to evaluate regeneration capacity. The mixture was stirred for 24 h at 25°C, as described in Section 2.4. After equilibration, the adsorbent was dried at 60°C for 12 h and then dispersed in 1 M HNO_3. The Pb(II)-loaded CBOMC-APD was treated with ultrasound and filtered, and the amount of desorbed Pb(II) was measured. After regeneration, the adsorbent was rinsed with DI water and used in subsequent adsorption experiments. The adsorption–desorption process was investigated in five cycles.

3. Results and discussion

3.1. Characterization of the adsorbents

Fig. 1 shows the N_2 adsorption–desorption isotherms and the corresponding pore size distribution of the

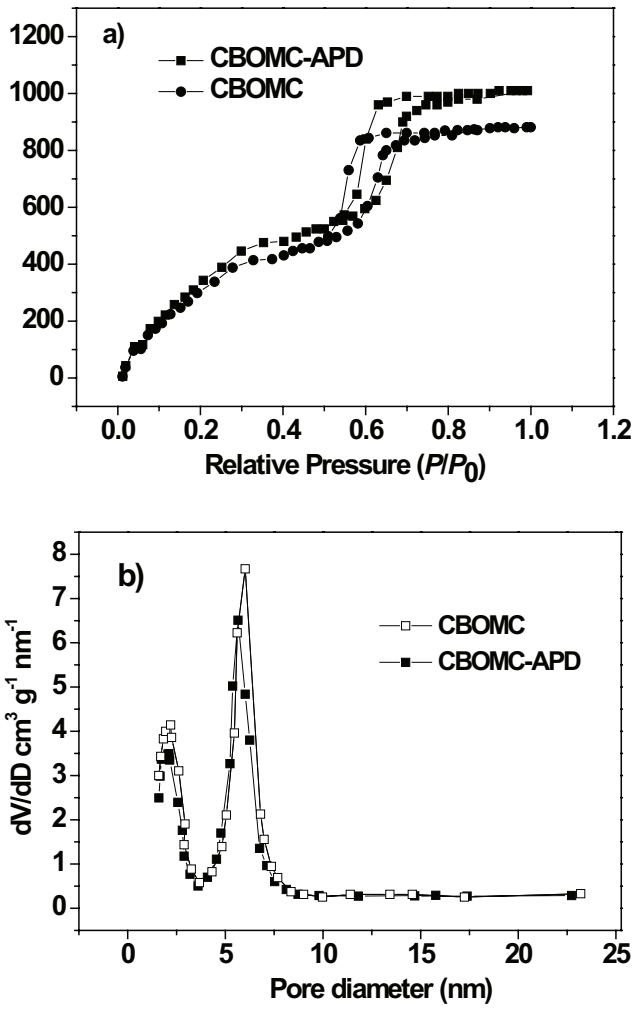

Fig. 1. N_2 adsorption isotherms (a) and pore size distribution curves (b) of CBOMC and CBOMC-APD.

pristine CBOMC and the modified CBOMC-APD particles. As shown in Fig. 1(a), the N_2 adsorption–desorption isotherms of CBOMC and CBOMC-APD exhibit similar type-IV curves with two evident capillary condensation steps ($0.1 < P/P_0 < 0.3$, $0.55 < P/P_0 < 0.70$), implying the existence of narrow pore size distributions of uniform cage-like mesopores at about 2–3 nm and 6–7 nm, respectively. The smaller pores with wide distributions below 3.0 nm are inside the pore walls because of the removal of silica from the carbon–silica composites. This result indicates that carbon and silica phases are separated and "homogeneously" distributed inside the pore walls on a nanoscale level. As shown in Fig. 1(b), the two most probable mesopore sizes are centered at 2.2 and 6.1 nm for the pristine CBOMC, and 2.1 and 5.6 nm for the modified CBOMC-APD by the BJH method, further confirming the bimodal-like mesopore size distribution of the two carbons. Calculated from the N_2 adsorption–desorption isotherms, the BET surface area and total pore volume are 2,308 $m^2 \cdot g^{-1}$ and 1.986 $cm^3 \cdot g^{-1}$ for the pristine CBOMC, and 2,021 $m^2 \cdot g^{-1}$ and 1.645 $cm^3 \cdot g^{-1}$ for the modified CBOMC-APD, respectively. The slight

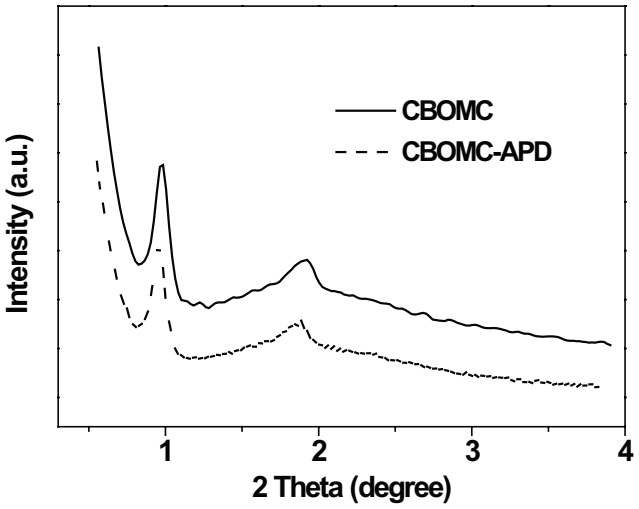

Fig. 2. SAXRD patterns of pristine CBOMC (a) and modified CBOMC-APD (b).

decrease in surface area, total pore volume, and pore size of the modified CBOMC-APD compared with those of the pristine CBOMC was due to the nitrogen-containing functional groups' occupation of pore volumes, which implied the successful introduction of amino groups on the CBOMC.

SAXRD was performed to measure the ordered degree of pore channels for the pristine CBOMC and modified CBOMC-APD. The diffraction profiles in Fig. 2 show evident (100) and (110) peaks for both samples, corresponding to a 2D hexagonal symmetry. After modification, the ordered structural regularity of the CBOMC-APD was well-reserved. More evidence was provided by the TEM images in large domains (Fig. 3). The CBOMC-APD maintained the ordered carbon framework and uniform pore channels similar to the parent counterpart, showing that no distinct damages were caused during the modification. This indicates that the acidic APS solution is a gentle oxidant that causes less destruction of bimodal ordered CBOMC framework compared with other strong oxidants like nitric acid. The latter usually deteriorates the structural regularity of ordered CBOMCs through the dissolution of carbon species [18]. The deterioration of pore structures usually results in the wet oxidation of CBOMC materials, which was not severe when APS was used as a gentle oxidant in this study. This property benefits the adsorption ability of the modified CBOMC-APD toward metal ions.

FT-IR spectroscopy was employed to examine the functional groups of the modified CBOMC-APD. By comparing the FTIR spectra of the modified CBOMC-APD to that of its pristine counterpart CBOMC (Fig. S1), new peaks at 1673, 1571, and 1021 cm^{-1} appeared, corresponding to the nitrogen-containing functional groups of $-NH_2$ and –RNH. According to the XPS spectra of CBOMC and CBOMC-APD presented in Fig. 4, carbon, oxygen, and nitrogen are the predominant elements observed on the surface of CBOMC-APD with binding energies of 285 eV (C 1s), 533 eV (O 1s), and 400.1 eV (N 1s). The N 1 s spectra of CBOMC-APD exhibited their maximum at BE = 400.1 eV with a shoulder around

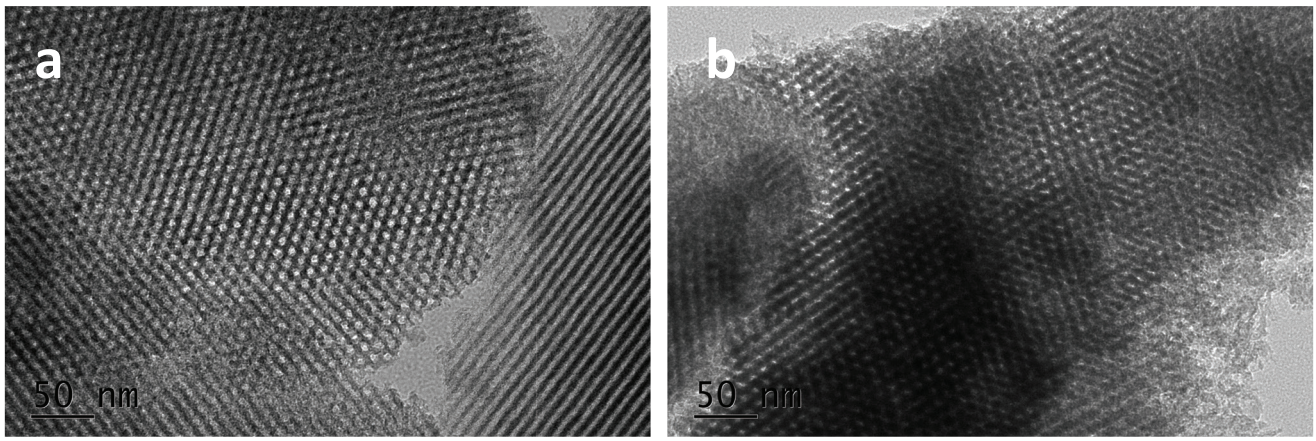

Fig. 3. TEM images of pristine CBOMC (a) and modified CBOMC-APD (b).

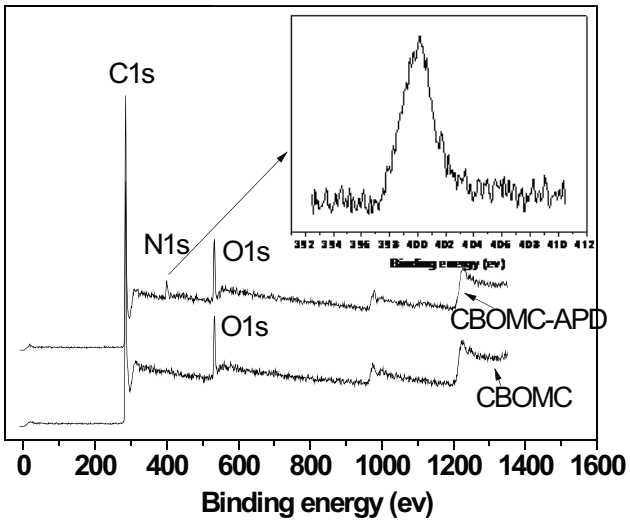

Fig. 4. XPS of CBOMC and CBOMC-APD before and after diethylenetriamine modification (insert image is the N1s spectra for CBOMC-APD).

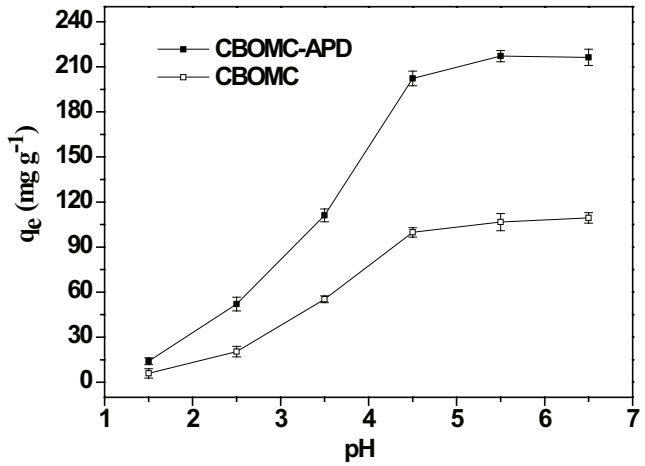

Fig. 5. The effect of solution pH on the adsorption of Pb(II).

399 eV (inset of Fig. 4). These signals could be assigned as the amino and imide function groups, respectively [32–34]. No nitrogen N 1s peaks were observed from the XPS spectra of the pristine CBOMC, although strong carbon and oxygen peaks appeared. The FTIR and XPS analyses confirmed that the amino groups were successfully introduced on CBOMC-APD after modification. This result was further demonstrated by the elemental analysis data. The nitrogen percentage of CBOMC-APD reaches 5.55%, whereas the concentration of pristine CBOMC is negligible. The amine group concentration is 3.96 mmol·g^{-1} for CBOMC-APD according to the elemental analysis data, which corresponds to the XPS results.

3.2. Effect of pH on Pb(II) adsorption

pH plays a key role in metal adsorption. At different pH values, the protonation and deprotonation of acidic and basic groups are influenced. To investigate the adsorption ability of CBOMC-APD for Pb(II), the effect of solution pH on the adsorption of Pb(II) ions onto CBOMC and CBOMC-APD is illustrated in Fig. 5. The adsorption of Pb(II) onto CBOMC-APD increased greatly at pH < 5.0 and remained stable as pH increased (Fig. 5). This finding shows that the solution pH remarkably affected the adsorption of Pb(II) onto the two carbons.

The main factors that affect pH on the adsorption process are probably associated with pH_{pzc} and speciation of lead in aqueous phase [35,36]. The pH_{pzc} of CBOMC-APD and CBOMC is 5.5 and 5.0, respectively. The surface of the adsorbents carried positive charge as solution pH < pH_{pzc} (Eq. (2)) and vice versa (Eq. (3)) as a result of the protonation reaction. The positively charged lead species were repelled by the positively charged carbon surface molecules when pH < pH_{pzc}, resulting in the decrease of Pb(II) adsorption along with pH value. The increase in pH resulted in more free available adsorption sites for Pb(II) adsorption because more H_3O^+ ions were liberated from the adsorbent's surface, as shown in Eq. (2). When the solution pH > pH_{pzc}, the surface of the adsorbent became negatively charged and favored Pb(II) adsorption (Eq. (5)), although the precipitation of lead oxide might also occur [36,37]. Although the solution pH has some effects on Pb(II) adsorption, the capacity is stable in the range of pH 4.5–6.5 for CBOMC-APD. In addition, the

Pb(II)-adsorbing capacity of the modified CBOMC-APD is always higher than that of the pristine CBOMC, suggesting that the modification favors for Pb(II) adsorption.

$$CBOMC–NH_3^+ \rightarrow CBOMC–NH_2+H^+ \quad (2)$$

$$CBOMC–NH_2 + H^+ \rightarrow CBOMC–NH_3^+ \quad (3)$$

$$CBOMC–NH_2 + Pb^{2+} \rightarrow CBOMC–NH_2–Pb^{2+} \quad (4)$$

$$CBOMC–NH_2 + OH^- \rightarrow CBOMC–NH_2OH^- \quad (5)$$

3.3. Effect of initial concentration

Fig. 6 shows the adsorption capacity and removal rate of CBOMC-APD for Pb(II) at different initial concentrations at 25°C. As observed from Fig. 6, the modified CBOMC-APD shows more excellent adsorption capacity for Pb(II) than the pristine CBOMC. More than 90% of Pb(II) ions was removed by CBOMC-APD as the Pb(II) concentration < 10 mg·L^{-1}, whereas only 40% of the Pb(II) was removed by CBOMC. The adsorption amount of the two materials significantly increased with increasing initial concentration. The amount of Pb(II) adsorbed by CBOMC-APD reached 302 mg·g^{-1} when the Pb(II) concentration was 70 mg·L^{-1}, which was nearly three times more than that the Pb(II) adsorbed by CBOMC (108 mg·g^{-1}). As the initial concentration increased, the removal rate of Pb(II) ions by CBOMC-APD remained at a high level even when the concentration reached 30 mg·g^{-1}. For instance, the removal rate of Pb(II) ions by CBOMC-APD was still higher than 70%, whereas the removal rate by CBOMC was less than 25%.

The amount of metal ions adsorbed on the porous material not only depends on the extent of diffusion inside the porous material but also on the chemical nature of the surface features (such as complexing capacity, steric effect, and hydrophilicity) [38–40]. As mentioned in Section 3.1, the specific surface area and pore volume of CBOMC-APD became smaller than CBOMC after chemical modification. However, the Pb(II) removal ability of CBOMC-APD turned far stronger than the pristine CBOMC, indicating that the modified amino groups on the material surface played a crucial role in Pb(II) adsorption.

3.4. Effect of temperature

Lead uptake as a function of temperature is shown in Fig. 7. The adsorption capacity of Pb(II) increased from 301 mg·g^{-1} to 377 mg·g^{-1} as temperature increased from 25°C to 45°C, suggesting that the adsorption process probably underwent a chemical instead of a physical interaction.

The adsorption potential energy (E) of the Pb(II) adsorption was estimated by the Dubinin–Kaganer–Radushkevich (D–K–R) equation [41].

$$\ln q_e = \ln q_m - \beta\varepsilon^2 \quad (6)$$

where q_e is the equilibrium adsorption capacity (mol·g^{-1}), q_m is the adsorption capacity on each monomolecular layer (mol·g^{-1}), β is the relative constant of the adsorption energy

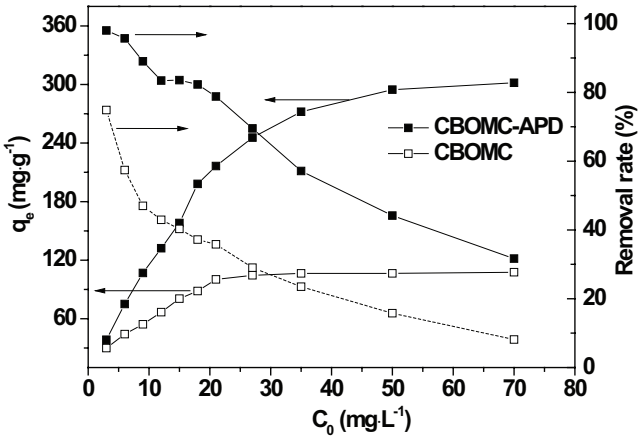

Fig. 6. Adsorption of Pb(II) and removal rate for CBOMC and CBOMC-APD.

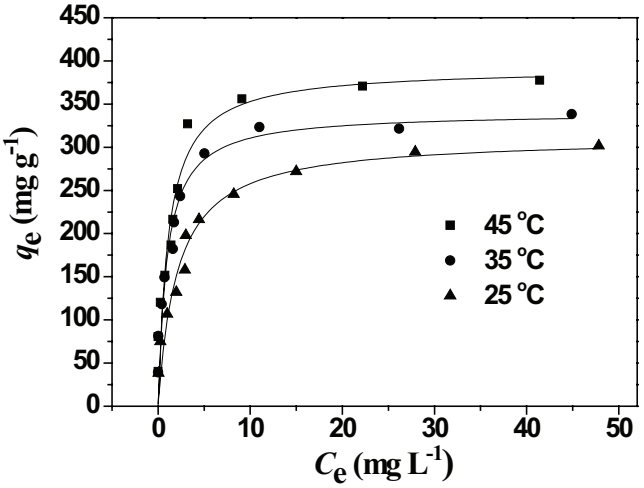

Fig. 7. Adsorption of Pb(II) on CBOMC-APD at different temperatures.

(mol^2·J^{-2}), and ε is the Polanyi adsorption potential. The form of ε is as follows:

$$\varepsilon = RT\ln(1/c_e) \quad (7)$$

where R is the gas constant (8.314J·(mol·K)$^{-1}$), T is the absolute temperature (K), and c_e is the equilibrium adsorption concentration (mol·g^{-1}). According to lnq_e and ε^2, the slope is the value and the adsorption capacity can be derived according to the intercept. According to the Hobson formula [41]:

$$E = -1/\sqrt{-2\beta}_T \quad (8)$$

where β and E meet the relational expression and E is the adsorption potential energy (kJ/mol).

The fitting results of the isothermal adsorption data through the D–K–R equation are shown in Table 1. The maximum adsorption capacity of the monomolecular layer increased along with temperature, implying that the

Table 1
Isotherm parameters of Pb(II) on CBOMC-APD at different temperatures

Isotherms	Parameters	Temperature (°C)		
		25°C	35°C	45°C
Langmuir	q^0 (mg·g^{-1})	311	339	391
$q_e = bq^0C_e/(1+bC_e)$	b (L·mg^{-1})	0.419	0.479	0.911
	R^2	0.948	0.916	0.905
Freundlich	K_F (L·mg^{-1})	128	178	198
$q_e = K_FC_e^{1/n}$	n	10	12	4.9
	R^2	0.917	0.904	0.896
Redlich–Peterson	K_F (L·mg^{-1})	288	469	378
$q_e = K_RC_e / (1+aCe^{\varrho})$	a_R (L·mg^{-1})	1.43	1.625	1.01
	ϱ	0.879	0.951	0.986
	R^2	0.912	0.909	0.893
Temkin	A_T (L·mg^{-1})	21	188	301
$y = \beta \ln A + B \ln x$	β_T (L·mg^{-1})	77	37	39
	R^2	0.939	0.910	0.868
Dubinin–Kaganer–	β_D (mol^2·J^{-2})	4.46E-09	3.00E-09	2.64E-09
Radushkevich	q_m (mg·g^{-1})	324	343	362
$\mathrm{Ln}q_e = \ln q_m - \beta\varepsilon^2$	R^2	0.975	0.954	0.933
	E (kJ·mol^{-1})	10.25	12.92	13.76

adsorption was an endothermic reaction and the increase in temperature promoted the adsorption. Adsorption potential energy in the ranges of 1–8 kJ·mol^{-1} and 9–16 kJ·mol^{-1} corresponds to the physical adsorption and chemical adsorption, respectively. The adsorption potential energies of lead on CBOMC-APD at 25°C, 35°C, and 45°C were all higher than 9 kJ·mol^{-1}, further confirming that the adsorption was a chemical reaction.

3.5. Isotherms and thermodynamic parameters

The isotherm experimental data were fitted with Langmuir, Freundlich, Redlich–Peterson, and Temkin isotherm models [42]. The calculated related parameters are listed in Table 1, and the different adsorption isotherms obtained are illustrated in Fig. S2. The adsorption experimental data of Pb(II) on the modified CBOMC-APD were well described using Langmuir isotherm model with the best correlation regression coefficients compared with Freundlich, Temkin, and Redlich–Peterson models. Moreover, the theoretical maximum adsorption capacity obtained by Langmuir model was highly approximate to the experimental results. The results mean that monolayer adsorption occurred on the CBOMC-APD surface with finite number of identical sites, which are homogeneously distributed over the adsorbent surface [19,42]. The Langmuir binding energy parameter b increased with increasing temperature, implying the adsorbent–adsorbate complexes formed during the adsorption process and higher temperature were more favorable to the adsorption.

The thermodynamic parameters including Gibbs free energy change (ΔG^0), enthalpy change (ΔH^0), and entropy change (ΔS^0) for Pb(II) adsorption were evaluated using the following equations:

Table 2
Adsorption thermodynamic parameters of Pb(II) on CBOMC-APD

T (°C)	ΔG^0 (kJ·mol^{-1})	ΔH^0 (kJ·mol^{-1})	ΔS^0 (kJ·mol^{-1}·K^{-1})
15	–16.45	93.17	0.370
25	–21.57	93.17	0.370
35	–22.26	93.17	0.370

$$\Delta G^\circ = -RT \ln K_D \quad (9)$$

$$\ln K_D = \Delta S^\circ / R - (\Delta H^\circ / R) / T \quad (10)$$

where R (8.314 J·(mol·K)$^{-1}$) and T (K) are the universal gas constant and the temperature in Kelvin, respectively. K_D is the adsorption equilibrium constant, and can be calculated by plotting lnK_D vs. q_e and extrapolating C_e to zero, where K_D was defined as q_e divided by C_e [43].

The ΔH^0 and ΔS^0 values obtained from the slope and intercept of Van't Hoff plots of $\mathrm{Ln}K_D$ vs. 1/T, respectively, and the ΔG^0 values at various temperatures are summarized in Table 2. The positive value of enthalpy change ΔH^0 indicated that the Pb(II) adsorption on CBOMC-APD was an endothermic process. Therefore, Pb(II) uptake increased along with temperature, which was in line with the previous analysis. In addition, enthalpy change ΔH^0 data are usually used to distinguish between physical and chemical adsorption. When the enthalpy change is larger than 40 kJ·mol^{-1}, the adsorption is typically associated with chemical adsorption [44,45]. The experimental enthalpy change was 93.17 kJ·mol^{-1}, implying that chemisorption dominated the adsorption of metal ions on CBOMC-APD [45]. The negative values of ΔG^0 ranged from −16.45 to −22.26, indicating that the adsorption of Pb(II) on CBOMC-APD was a feasible and spontaneous process. The decrease in ΔG^0 with increasing temperature demonstrated that the adsorption was more effective at higher temperatures. Meanwhile, the positive values of ΔS^0 indicated that the degrees of freedom increased at the solid solution interface during the adsorption of Pb(II) on CBOMC-APD, which reflected the spontaneity and affinity of the sorbents for Pb(II) ions.

3.6. Adsorption kinetics

The adsorption kinetics of Pb(II) at different concentrations were investigated to understand the adsorption behavior of the CBOMC-APD, as illustrated in Fig. 8. The adsorption process can be divided into two steps. The adsorption rate was considerably fast within the first 30 min, which may be due to the large number of available active sites on the surface of mesoporous CBOMC-APD. However, the adsorption rate was slow in the subsequent steps, and equilibrium capacity reached within 60 min. The equilibrium time for Pb(II) on the mesoporous CBOMC-APD in this study was much shorter than

that on epichlorohydrin-triphosphate and crosslinked carboxymethyl-chitosan resin [46,47]. This result indicates that the ordered mesoporous structure of the adsorbent favored the fast mass transfer of Pb(II).

To evaluate the kinetic adsorption mechanism, the pseudo-first-order, pseudo-second-order, and Elovich models were used to test the kinetic parameters. The values of the kinetic parameters and the correlation coefficients for Pb(II) adsorption at three different initial concentrations of 10, 20, and 30 mg·L^{-1} were obtained through non-linear regression and are listed in Table 3. Different adsorption kinetic fitting curves obtained at different concentrations are illustrated in Fig. S3. Compared with the Lagergren and Elovich kinetic models, the correlation coefficient values for the second-order kinetic model were higher for all Pb(II) concentrations, and its calculated equilibrium adsorption capacity $q_{e,cal}$ agrees with the experimental data.

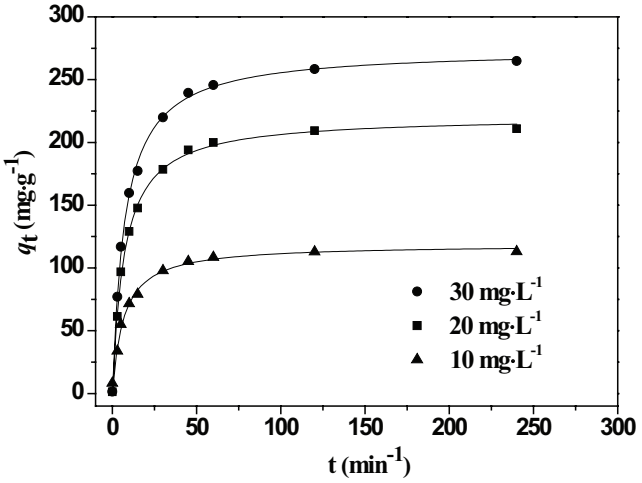

Fig. 8. Adsorption kinetics curve of Pb(II) on CBOMC-APD.

Table 3
Adsorption kinetics parameters of Pb(II) on CBOMC-APD

Models	Parameters	Concentration (mg·L^{-1})		
		10	20	30
Pseudo-first order	K_1 (min^{-1})	0.111	0.105	0.102
	R^2	0.969	0.980	0.976
$q_t = q_e - q_e e^{-k_1 t}$	$q_{e,ca}$ (mg·g^{-1})	108	200	248
	$q_{e,mea}$ (mg·g^{-1})	101	211	267
Pseudo-second order	K_2 (g·mg^{-1}·min^{-1})	1.28E-03	6.43E-04	4.98E-04
	R^2	0.989	0.998	0.998
$q_t = k_2 q_e^2 t / (1+k_2 q_e t)$	$q_{e,ca}$ (mg·g^{-1})	119	221	274
	$q_{e,mea}$ (mg·g^{-1})	101	211	267
Elovich	α_E (mg·g^{-1}·min^{-1})	76	122	140
$q_t = (1/\beta_E)$	β_E (g·min·mg^{-1})	0.0539	0.0283	0.0225
$\ln(\alpha_E\beta_E) + (1/\beta_E)\ln t$	R^2	0.938	0.954	0.938

This result suggests that the pseudo-second-order adsorption mechanism was predominant, and that the overall rate of Pb(II) adsorption was controlled by the chemisorption or chemical adsorption. The result also indicates that the adsorption of Pb(II) ions on the adsorbent probably proceeded through surface exchange reactions until the surface vacant sites were fully occupied; afterward, the Pb(II) ions may have diffused into the adsorbent's inner area for further interactions.

3.7. Adsorption mechanisms

3.7.1. Inhibition of diffusional mass transfer into the mesopores

The mechanism involved in the adsorption of Pb(II) on the modified CBOMC-APD was investigated [48]. The intraparticle diffusion model by Weber and Morris, which provided the rate for intraparticle diffusion, was applied to investigate the adsorption process [49]:

$$q_t = k_i t^{1/2} + C_i \quad (11)$$

where k_i (mg·g min$^{1/2}$) is the intraparticle diffusion rate constant and C_i is associated with the boundary layer thickness.

Fig. 9 shows the plots of q_t vs. $t^{0.5}$ at three different Pb(II) initial concentrations. The values of k_i and C_i obtained from the plots are summarized in Table 4. In all cases, the plots have the same general features and consist of two straight lines, depicting the mass transfer of lead ions from the solution to the CBOMC-APD. The adsorption trend lines did not pass the origin, which indicates that intraparticle diffusion was not the rate-limiting step in the adsorption process. The first steep-sloped period was the instantaneous diffusion stage (k_{i1}), during which a large amount of lead ions were rapidly adsorbed by the exterior surface of the adsorbent. When the adsorption of the exterior surface reached saturation, Pb(II) ions entered into the mesopores of the adsorbent

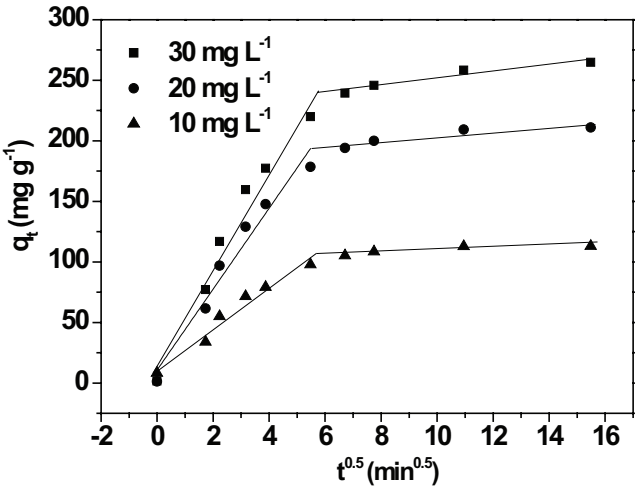

Fig. 9. Intra-particle models for Pb(II) adsorption kinetics on CBOMC-APD.

Table 4
Results from linear regression of intraparticle diffusion equation plots

C_0 (mg·L^{-1})	K_{i1} (mg·g^{-1}min$^{-1/2}$)	Equation	R_1^2	K_{i2} (mg·g^{-1}min$^{-1/2}$)	Equation	R^2
10	16.97	$q_t = 16.97t^{0.5} + 11.06$	0.958	0.828	$q_t = 0.828t^{0.5} + 101$	0.620
20	33.38	$q_t = 33.38t^{0.5} + 10.79$	0.956	1.832	$q_t = 1.832t^{0.5} + 185$	0.729
30	40.84	$q_t = 27.49t^{0.5} + 13.19$	0.961	2.824	$q_t = 2.824t^{0.5} + 223$	0.885

through the interior surface. The adsorption diffusion rate k_{i2} was slower than k_{i1} in all cases because of the increase of diffusion resistance as the Pb(II) ions entered into the pores. Nearly 95% of the adsorption occurred in the first stage with higher diffusion rate k_{i1}, suggesting that the use of mesoporous CBOMC-APD could provide faster Pb(II) removal by adsorption. Similar results were also obtained for stabilized landfill leachate treatment by Singh and Townsend [50].

3.7.2. Chemical reaction mechanism

The Pb(II) capacity of modified CBOMC-APD, as discussed in the previous section, is nearly twice more than that of the pristine CBOMC. However, the surface area, total pore volume, mesopore volume, and micropore volume of the CBOMC-APD are smaller than those of the pristine CBOMC, whereas the average pore size of the two adsorbents is close. Therefore, the enhanced Pb(II) adsorption capacity of the modified CBOMC-APD is ascribed to chemical binding rather than physical adsorption.

The surface properties of CBOMC-APD after absorbing Pb(II) were studied using XPS to investigate the chemical reaction of Pb(II) with the amino groups on CBOMC-APD. Compared with the XPS spectrum for CBOMC-APD before Pb(II) adsorption, two new peaks at 170 and 680 eV were observed for CBOMC-APD after Pb(II) adsorption, suggesting that Pb(II) ions were successfully adsorbed on the surface of CBOMC-APD (Fig. 10). Furthermore, the N 1s peak of CBOMC-APD after Pb(II) adsorption significantly shifted to the right, which confirms that a reaction occurred between CBOMC-APD and Pb (II) ions. These results show that the amino groups played an important role in the adsorption process.

According to Pearson's theory of hard and soft acid-base [51], the surface of the modified CBOMC-APD was made of weak bases with a pair of electrons on the nitrogen atom, whereas the Pb (II) was a soft acid. A covalent bond would be formed by the lone electron pair and the Pb vacant orbital. The amino groups were more prone to combine with Pb(II) ions and produce mono-amine or di-amine lead compounds at normal conditions. This phenomenon enabled Pb(II) adsorption on the surface of the MC through the functional groups to form a stable state of chemical adsorption.

3.8. Regeneration

Examining the performance of adsorbents through simulated adsorption/desorption cycles is important to assess their reusability and cost effectiveness. As described in Section 3.2, the CBOMC-APD surface was protonated by H_3O^+ ions under acidic conditions to facilitate Pb(II) desorption. The competition of H^+ ions in the adsorption sites promoted the release of the adsorbed Pb(II) into the aqueous solution, indicating that acid treatment may be a feasible approach for regeneration. Regeneration and adsorption by 1.0 mol L^{-1} HNO_3 were repeated five times. Fig. S4 shows the results of five adsorption–regeneration cycles of Pb(II) on sample CBOMC-APD. The removal efficiency was still higher than 96% after five adsorption–regeneration cycles, indicating that HNO_3 is an effective desorption effluent and the synthesized CBOMC-APD adsorbent is rather reusable. The developed CBOMC-APD adsorbent showed excellent properties for the removal of Pb(II) from aqueous solutions, including high adsorption capacities, fast uptake rates, and high reusability. These properties display a good prospect for practical applications in the removal of Pb(II) from wastewater.

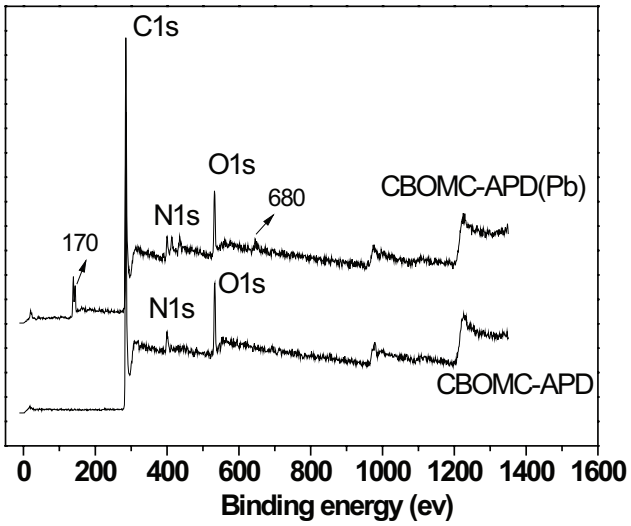

Fig. 10. XPS of CBOMC and CBOMC-APD before and after Pb(II) adsorption.

3.9. Comparison of the Pb(II)-adsorbing performance of CBOMC-APD with literature data

The Pb(II)-removing capacity of CBOMC-APD adsorbent was compared with different adsorbents reported in literature [3–7,36,47,48], as summarized in Table 5. Comparison of the maximum adsorption amount (q_{max}) values showed

Table 5
Comparison of maximum adsorption capacities (q_{max}) of Pb(II)

Sorbents	q_{max} (mg g^{-1})	Reference
Water treatment residual	21.73	[3]
Xanthate-modified apple pomace	178	[4]
Iron-oxide-immobilized sand	11.30	[5]
H_3PO_4-activated cotton stalk carbon	119	[6]
Sporopollenin biomass	6.10	[7]
Polygonum orientale Linn AC	98.39	[36]
Epichlorohydrin-triphosphate-modified chitosan	166.94	[47]
N-MSU-F-S/Fe_3O_4	222.4	[48]
CBOMC-APD	391	This study

that the adsorption efficiency of the CBOMC-APD prepared in our work was generally higher than previously reported values. The high adsorption efficiency of the CBOMC-APD is probably because of the bimodal-ordered mesopores and the introduced functional groups on the MC (synergistic effect), which confirm that the CBOMC-APD could be used as a good adsorbent.

4. Conclusions

We presented a comprehensive study on surface chemistry, textural properties of modified bimodal-ordered MC, and Pb(II) adsorption behavior. First, bimodal-ordered OMC with large specific surface area and bimodal ordered pore channel was prepared based on a soft template method, i.e., EISA, followed by wet modification using APD. The modified CBOMC-APD maintained rich bimodal-ordered mesopores, which means that the modification of APD introduced large number of amino groups to the bimodal-ordered MC without changing the ordered structure of the pore. The introduced amine group concentration was up to 3.96 mmol·g^{-1} for the modified CBOMC-APD, indicating that the bimodal-ordered system was more likely to graft surface groups. The Langmuir adsorption capacity of the modified carbon reached 391 mg·g^{-1}, and almost 80% of Pb(II) was removed by the modified CBOMC-APD in 30 min. The adsorption performance remained stable even at pH 4.5, when initial Pb(II) concentration and temperature had significant influence on the adsorption capacity. The Pb(II) was combined with the amino groups through strong complexation, which resulted in high pH stability, as shown by the comparison of XPS analyses before and after adsorption. Overall, the findings in this study not only further confirmed that the high adsorption ability is up to the combined effects of pore structures and amino function groups but also demonstrated the suitability of co-assembled CBOMC with high surface area for preparing amino-functionalized bimodal OMC with high surface area for Pb(II), as well as other divalent alkaline earth metal ions.

Acknowledgments

The authors acknowledge the research grants provided by China under the Natural Science Foundation (No. 51102136), the Fundamental Research Funds for the Central Universities (No. 2015NJAUG02) and China Postdoctoral Science Fund (No. 2014M560429).

References

[1] A. Guittonny-Philippe, V. Masotti, P. Hohener, J.L. Boudenne, J. Viglione, I. Laffont-Schwob, Constructed wetlands to reduce metal pollution from industrial catchments in aquatic Mediterranean ecosystems: a review to overcome obstacles and suggest potential solutions, Environ. Int., 64 (2014) 1–16.
[2] G.X. Yang, H. Jiang, Amino modification of biochar for enhanced adsorption of copper ions from synthetic wastewater, Water Res., 48 (2014) 396–405.
[3] P. Castaldi, M. Silvetti, G. Garau, D. Demurtas, S. Deiana, Copper(II) and lead(II) removal from aqueous solution by water treatment residues, J. Hazard. Mater., 283 (2015) 140–147.
[4] P. Chand, A. Bafana, Y.B. Pakade, Xanthate modified apple pomace as an adsorbent for removal of Cd (II), Ni (II) and Pb (II), and its application to real industrial wastewater, Int. Biodeterior. Biodegrad., 97 (2015) 60–66.
[5] S.M. Lee, C. Laldawngliana, D. Tiwari, Iron oxide nanoparticles-immobilized-sand material in the treatment of Cu(II), Cd(II) and Pb(II) contaminated waste waters, Chem. Eng. J., 195 (2012) 103–111.
[6] M. Raii, D.P. Minh, F.J.E. Sanz, A. Nzihou, Lead and cadmium removal from aqueous solution using an industrial gypsum by-product, Proc. Eng., 83 (2014) 415–422.
[7] M. Sener, D.H.K. Reddy, B. Kayan, Biosorption properties of pretreated sporopollenin biomass for lead(II) and copper(II): application of response surface methodology, Ecol. Eng., 68 (2014) 200–208.
[8] P.A. Xu, G.M. Zeng, D.L. Huang, C.L. Feng, S. Hu, M.H. Zhao, C. Lai, Z. Wei, C. Huang, G.X. Xie, Z.F. Liu, Use of iron oxide nanomaterials in wastewater treatment: a review, Sci. Total Environ., 424 (2012) 1–10.
[9] J.L. Gong, B. Wang, G.M. Zeng, C.P. Yang, C.G. Niu, Q.Y. Niu, W.J. Zhou, Y. Liang, Removal of cationic dyes from aqueous solution using magnetic multi-wall carbon nanotube nanocomposite as adsorbent, J. Hazard. Mater., 164 (2009) 1517–1522.
[10] R. Tovar-Gomez, M.D. Moreno-Virgen, J. Moreno-Perez, A. Bonilla-Petriciolet, V. Hernandez-Montoya, C.J. Duran-Valle, Analysis of synergistic and antagonistic adsorption of heavy metals and acid blue 25 on activated carbon from ternary systems, Chem. Eng. Res. Des., 93 (2015) 755–772.
[11] L. Brown, K. Seaton, R. Mohseni, A. Vasiliev, Immobilization of heavy metals on pillared montmorillonite with a grafted chelate ligand, J. Hazard. Mater., 261 (2013) 181–187.
[12] M. Ceglowski, G. Schroeder, Preparation of porous resin with Schiff base chelating groups for removal of heavy metal ions from aqueous solutions, Chem. Eng. J., 263 (2015) 402–411.
[13] Y.Y. Ge, X.M. Cui, Y. Kong, Z.L. Li, Y. He, Q.Q. Zhou, Porous geopolymeric spheres for removal of Cu(II) from aqueous solution: synthesis and evaluation, J. Hazard. Mater., 283 (2015) 244–251.
[14] G.P. Hao, W.C. Li, S.A. Wang, S.F. Zhang, A.H. Lu, Tubular structured ordered mesoporous carbon as an efficient sorbent for the removal of dyes from aqueous solutions, Carbon, 48 (2010) 3330–3339.
[15] G. Wang, B.J. Dou, Z.S. Zhang, J.H. Wang, H.E. Liu, Z.P. Hao, Adsorption of benzene, cyclohexane and hexane on ordered mesoporous carbon, J. Environ. Sci., 30 (2015) 65–73.
[16] K.Q. Li, Y. Jiang, X.H. Wang, D. Bai, H. Li, Z. Zheng, Effect of nitric acid modification on the lead(II) adsorption of mesoporous biochars with different mesopore size distributions, Clean Technol. Environ. Policy, 18 (2016) 797–805.

[17] K. Li, J. Li, M. Lu, H. Li, X. Wang, Preparation and amino modification of mesoporous carbon from bagasse via microwave activation and ethylenediamine polymerization for Pb(II) adsorption, Desal. Wat. Treat., 57 (2016) 24004–24018. DOI: 10.1080/19443994.20 16 .1138891.
[18] X.X. Dai, F.G. Qiu, X. Zhou, Y.M. Long, W.F. Li, Y.F. Tu, Amino-functionalized mesoporous silica modified glassy carbon electrode for ultra-trace copper(II) determination, Anal. Chim. Acta, 848 (2014) 25–31.
[19] W. Shan, Y. Shu, H. Chen, D. Zhang, W. Wang, H. Ru, Y. Xiong, The recovery of molybdenum(VI) from rhenium(VII) on amino-functionalized mesoporous materials, Hydrometallurgy, 165 (2016) 251–260. DOI: 10.1016/j.hydromet.2016.02.005.
[20] W.J. Yang, P. Ding, L. Zhou, J.G. Yu, X.Q. Chen, F.P. Jiao, Preparation of diamine modified mesoporous silica on multi-walled carbon nanotubes for the adsorption of heavy metals in aqueous solution, Appl. Surf. Sci., 282 (2013) 38–45.
[21] M. Hadavifar, N. Bahramifar, H. Younesi, Q. Li, Adsorption of mercury ions from synthetic and real wastewater aqueous solution by functionalized multi-walled carbon nanotube with both amino and thiolated groups, Chem. Eng. J., 237 (2014) 217–228.
[22] M.H. Mahaninia, P. Rahimian, T. Kaghazchi, Modified activated carbons with amino groups and their copper adsorption properties in aqueous solution, Chin. J. Chem. Eng., 23 (2015) 50–56.
[23] X.B. Wang, J. Liu, W.Z. Xu, One-step hydrothermal preparation of amino-functionalized carbon spheres at low temperature and their enhanced adsorption performance towards Cr(VI) for water purification, Colloid. Surface A., 415 (2012) 288–294.
[24] Z.Z. Guo, J.L. Fan, J. Zhang, Y. Kang, H. Liu, L. Jiang, C.L. Zhang, Sorption heavy metal ions by activated carbons with well-developed microporosity and amino groups derived from *Phragmites australis* by ammonium phosphates activation, J. Taiwan Inst. Chem. Eng., 58 (2016) 290–296.
[25] L.L. Jiang, S.J. Li, H.T. Yu, Z.S. Zou, X.G. Hou, F.M. Shen, C.T. Li, X.Y. Yao, Amino and thiol modified magnetic multi-walled carbon nanotubes for the simultaneous removal of lead, zinc, and phenol from aqueous solutions, Appl. Surf. Sci., 369 (2016) 398–413.
[26] E.G. Lemraski, Z. Palizban, Comparison of 2-amino benzyl alcohol adsorption onto activated carbon, silicon carbide nanoparticle and silicon carbide nanoparticle loaded on activated carbon, J. Mol. Liq., 212 (2015) 245–258.
[27] M. Barczak, K. Michalak-Zwierz, K. Gdula, K. Tyszczuk-Rotko, R. Dobrowolski, A. Nbrowski, Ordered mesoporous carbons as effective sorbents for removal of heavy metal ions, Microporous Mesoporous Mater., 211 (2015) 162–173.
[28] P.A. Bazula, A.H. Lu, J.J. Nitz, F. Schuth, Surface and pore structure modification of ordered mesoporous carbons via a chemical oxidation approach, Microporous Mesoporous Mater., 108 (2008) 266–275.
[29] R.X. Guo, J. Guo, F.Q. Yu, D.D. Gang, Synthesis and surface functional group modifications of ordered mesoporous carbons for resorcinol removal, Microporous Mesoporous Mater., 175 (2013) 141–146.
[30] A. Sanchez-Sanchez, F. Suarez-Garcia, A. Martinez-Alonso, J.M.D. Tascon, Surface modification of nanocast ordered mesoporous carbons through a wet oxidation method, Carbon, 62 (2013) 193–203.
[31] R.L. Liu, Y.F. Shi, Y. Wan, Y. Meng, F.Q. Zhang, D. Gu, Z.X. Chen, B. Tu, D.Y. Zhao, Triconstituent co-assembly to ordered mesostructured polymer-silica and carbon-silica nanocomposites and large-pore mesoporous carbons with high surface areas, J. Am. Chem. Soc., 128 (2006) 11652–11662.
[32] F. Ran, J. Li, Y. Lu, L.R. Wang, S.Q. Nie, H.M. Song, L. Zhao, S.D. Sun, C.S. Zhao, A simple method to prepare modified polyethersulfone membrane with improved hydrophilic surface by one-pot: the effect of hydrophobic segment length and molecular weight of copolymers, Mat. Sci. Eng. C-Mat., 37 (2014) 68–75.
[33] R.J.J. Jansen, H. Vanbekkum, XPS of nitrogen-containing functional-groups on activated carbon, Carbon, 33 (1995) 1021–1027.
[34] G. Yang, H.L. Chen, H.D. Qin, Y.J. Feng, Amination of activated carbon for enhancing phenol adsorption: effect of nitrogen-containing functional groups, Appl. Surf. Sci., 293 (2014) 299–305.
[35] D. Bozic, M. Gorgievski, V. Stankovic, N. Strbac, S. Serbula, N. Petrovic, Adsorption of heavy metal ions by beech sawdust – kinetics, mechanism and equilibrium of the process, Ecol. Eng., 58 (2013) 202–206.
[36] L. Wang, J. Zhang, R. Zhao, Y. Li, C. Li, C.L. Zhang, Adsorption of Pb(II) on activated carbon prepared from Polygonum orientale Linn.: kinetics, isotherms, pH, and ionic strength studies, Bioresour. Technol., 101 (2010) 5808–5814.
[37] I. Ghorbel-Abid, M. Trabelsi-Ayadi, Competitive adsorption of heavy metals on local landfill clay, Arab. J. Chem., 8 (2015) 25–31.
[38] D.M. Burke, M.A. Morris, J.D. Holmes, Chemical oxidation of mesoporous carbon foams for lead ion adsorption, Sep. Purif. Technol., 104 (2013) 150–159.
[39] K. Zhang, W.H. Cheung, M. Valix, Roles of physical and chemical properties of activated carbon in the adsorption of lead ions, Chemosphere, 60 (2005) 1129–1140.
[40] W.H. Zhang, L.W. Zhuang, Y.A. Yuan, L.Z. Tong, D.C.W. Tsang, Enhancement of phenanthrene adsorption on a clayey soil and clay minerals by coexisting lead or cadmium, Chemosphere, 83 (2011) 302–310.
[41] F.C. Wu, R.L. Tseng, R.S. Juang, Initial behavior of intraparticle diffusion model used in the description of adsorption kinetics, Chem. Eng. J., 153 (2009) 1–8.
[42] A. Murugesan, L. Ravikumar, V. Sathya Selva Bala, P. Senthil Kumar, T. Vidhyadevi, S.D. Kirupha, S.S. Kalaivani, S. Krithiga, S. Sivanesan, Removal of Pb(II), Cu(II) and Cd(II) ions from aqueous solution using polyazomethineamides: equilibrium and kinetic approach, Desalination, 271 (2011) 199–208.
[43] M. Xing, J. Wang, Nanoscaled zero valent iron/graphene composite as an efficient adsorbent for Co(II) removal from aqueous solution, J. Colloid Interface Sci., 474 (2016) 119–128.
[44] N. Rauf, S.S. Tahir, J.H. Kang, Y.S. Chang, Equilibrium, thermodynamics and kinetics studies for the removal of alpha and beta endosulfan by adsorption onto bentonite clay, Chem. Eng. J., 192 (2012) 369–376.
[45] A.P. Terzyk, G. Rychlicki, The influence of activated carbon surface chemical composition on the adsorption of acetaminophen (paracetamol) in vitro - the temperature dependence of adsorption at the neutral pH, Colloid. Surface. A, 163 (2000) 135–150.
[46] S.L. Sun, L. Wang, A.Q. Wang, Adsorption properties of crosslinked carboxymethyl-chitosan resin with Pb(II) as template ions, J. Hazard. Mater., 136 (2006) 930–937.
[47] R. Laus, T.G. Costa, B. Szpoganicz, V.T. Favere, Adsorption and desorption of Cu(II), Cd(II) and Pb(II) ions using chitosan crosslinked with epichlorohydrin-triphosphate as the adsorbent, J. Hazard. Mater., 183 (2010) 233–241.
[48] J. Chung, J. Chun, J. Lee, S.H. Lee, Y.J. Lee, S.W. Hong, Sorption of Pb(II) and Cu(II) onto multi-amine grafted mesoporous silica embedded with nano-magnetite: effects of steric factors, J. Hazard. Mater., 239 (2012) 183–191.
[49] W.J. Weber, J.C. Morris, Kinetics of adsorption on carbon from solution, J. San. Eng. Div. ASCE., 89 (1963) 31–59.
[50] S.K. Singh, T.G. Townsend, D. Mazyck, T.H. Boyer, Equilibrium and intra-particle diffusion of stabilized landfill leachate onto micro- and meso-porous activated carbon, Water Res., 46 (2012) 491–499.
[51] P. Hadi, M.H. To, C.W. Hui, C.S.K. Lin, G. McKay, Aqueous mercury adsorption by activated carbons, Water Res., 73 (2015) 37–55.

Supplementary data

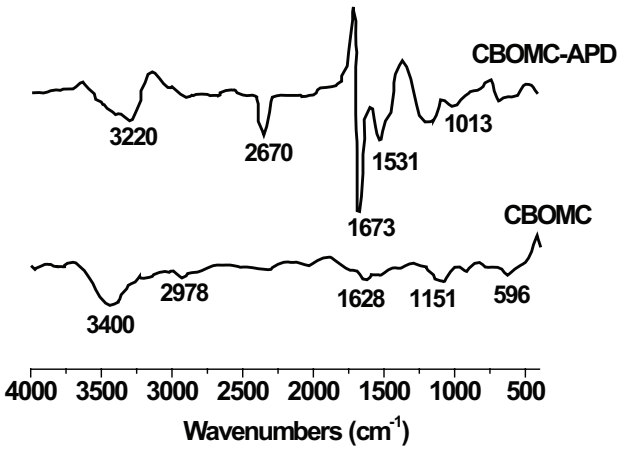

Fig. S1. FT-IR spectra of pristine and modified CBOMC.

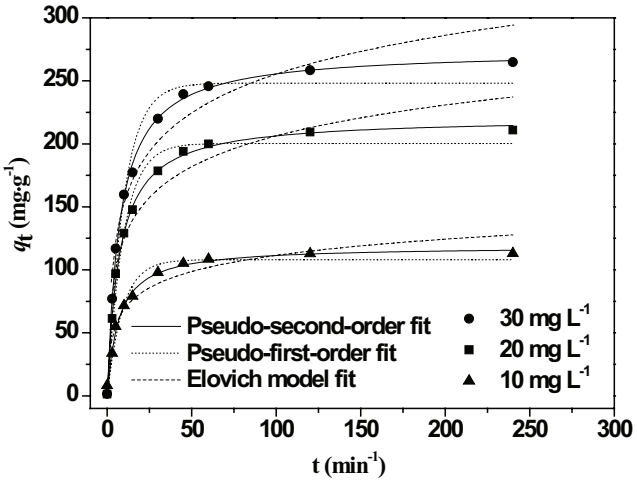

Fig. S3. Comparison of different kinetic models for Pb(II) on CBOMC-APD at different temperatures.

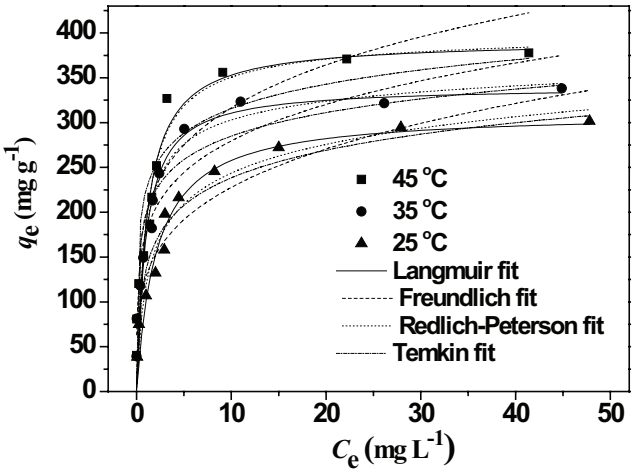

Fig. S2. Comparison of different isotherm models for Pb(II) on CBOMC-APD at different temperatures.

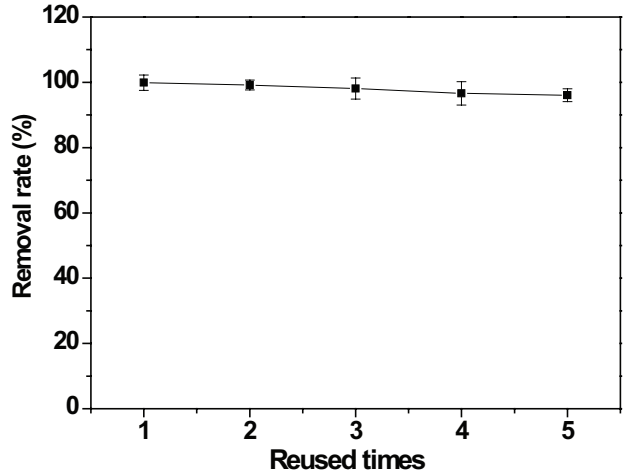

Fig. S4. Removal rate of Pb(II) on CBOMC-APD as a function of the reused times.